https://dx.doi.org/10.21577/0103-5053.20220130

J. Braz. Chem. Soc., Vol. 34, No. 5, 641-652, 2023

Article

The Use of Single Crystal X-ray Diffraction Technique for Characterization of 25I-NBOMe and 25R-NBOH (R = Cl, I, Br, Et) in Forensic Application

Maria C. C. Lucena,[a] Karen P. S. Lopes,[b] Alejandro P. Ayala,[c] Laura M. T. Vidal,[d] Thiago I. B. Lopes[a] and Nágila M. P. S. Ricardo [*,b]*

[a]*Polícia Federal, 60415-510 Fortaleza-CE, Brazil*

[b]*Laboratório de Polímeros e Inovação de Materiais (LabPIM), Departamento de Química Orgânica e Inorgânica, Centro de Ciências, Universidade Federal do Ceará, 60455-760 Fortaleza-CE, Brazil*

[c]*Departamento de Física, Centro de Ciências, Universidade Federal do Ceará, 60440-900 Fortaleza-CE, Brazil*

[d]*Departamento de Farmácia, Faculdade de Farmácia, Odontologia e Enfermagem, Universidade Federal do Ceará, 60430-355 Fortaleza-CE, Brazil*

Criminal minds create new psychoactive substances (NPS) to dribble the Drug Regulatory System. Early Warning Systems (EWA) were instituted worldwide to combat this practice. Brazilian government has started establishing EWA at a national level since August 2021. The role of drug analysis laboratories in EWA is very important and experts working at forensic laboratories are in the main position to detect NPS and any changes in the molecular structures. However, for this practice, it is necessary to use reliable analyses techniques for unequivocal identification. The goal of this work is to use single-crystal X-ray diffraction (XRD) to detect the presence of NPS and elucidate its molecular structure using single crystals from a seized blotter paper. XRD is also useful to prepare reference substances to produce entries to be included in Fourier transformed infrared spectroscopy (FTIR) and mass spectrometry databases, which are some of the most relevant routine techniques in forensic laboratories. This approach was used to study the NPS 25R-NBOH and 25I-NBOMe using XRD, FTIR, Raman, and nuclear magnetic resonance spectroscopies. The results showed that molecular structure methods must be used to elucidate NPS in an unambiguous manner and the potential of XRD use in the forensic area as a reference method.

Keywords: single-crystal X-ray diffraction, 25R-NBOH, 25I-NBOMe, NMR, Raman, ATR-FTIR

Introduction

According to the United Nations Office on Drugs and Crime (UNODC) Synthetic Drug Strategy 2021-2025 Report,[1] the number of new psychoactive substances (NPS) emerging on illicit drug markets has a six-fold increase in the past decade and reached a record level of over 1,000 unique substances in 2020. In addition, annual global seizures of amphetamine-type stimulants increased by 64% in 2019, while opioid use disorder deaths have gone up by 71% over the past decade.

The family of 2-(4-R-2,5-dimethoxyphenyl)-*N*-[(2-hydroxyphenyl)methyl] ethanamine (25R-NBOH, with R being a halogen or an alkyl group) is emerging as lysergic acid diethylamide (LSD) alternatives in the illicit drug market.[2]

In Brazil, the benzylphenethylamine group accounted, in 2019,[3] for 35.7% of NPS Federal Police (FP) reports, an increase over 2018 (15.7%), a smaller prevalence than in 2016 and 2017 (26.5 and 42.4%). In 2018, the most prevalent substances of the benzylphenethylamine group were: 25C-NBOH, 25E-NBOH, 25H-NBOH, and *N*-acetyl 25I-NBOMe.[4]

There are many reports in Police Departments about blotter papers seizures containing *N*-benzylphenethylamines derivatives, such as NBOMe and NBOH. 25R-NBOMe ((4-R-2,5-dimethoxyphenethyl) (2-methoxybenzyl) amine) and 25R-NBOH ((4-R-2,5-dimethoxyphenethyl) (2-hydroxybenzyl)amine), where R could be either Cl, Br,

*e-mail: naricard@ufc.br
Editor handled this article: Fernando C. Giacomelli (Associate)

I or an organic substituent. Both of them are synthetic drug families included in the benzylphenethylamines class.[5-8]

The NBOH group are still considered NPS,[9,10] since they are not internationally controlled by the United Nations 1961 or 1971 conventions yet,[11] nevertheless, that is not the case of 25I-NBOMe which was included in 2015 in the list of the 1971's Convention.[12]

There is a challenge in identifying and quantifying new NBOMe and NBOH because the forensic laboratories do not have easy access to NPS analytical standards. Even when analytical standards are available, they are very expensive, and the delivery time is always long due to the need for import authorization from Drugs Control Institutions. In the case of NBOMe and NBOH, access is even harder because the NPS reference standards are not globally marketed.[13]

Single-crystal X-ray diffraction (SCXRD) has been applied in designed drugs with success for forensic purposes.[14,15] Since 2010, Nycz *et al.*[16] have studied and identified some synthetic cannabinoids by X-ray diffraction, and in 2011 applied this technique supported by computational tools to ascertain the atomic charges of selected cathinones, the energy of the frontier orbitals, and the conformational of groups, which have not been determined by crystallographic studies yet. The identification of cathinones is of medical and forensic or doping interest.[17] In 2021, Barros *et al.*[13] reported the single-crystal X-ray diffraction of hydrochloride derivatives of three synthesized NBOHs (25H-, 25I- and 25B-NBOH).

Spectroscopic analysis such as Fourier transform infrared spectroscopy (FTIR) and gas chromatography-mass spectrometry (GC-MS) are routine techniques in forensic laboratories,[8] however, for NPS elucidative characterization, the experts have included complementary techniques such as nuclear magnetic resonance (NMR) and Raman spectroscopies. Pereira *et al.*[18] used Fourier transform infrared using attenuated total reflectance (ATR-FTIR) and multivariate discriminant analysis to classify NPS in seized blotter papers, and Piorunska-Sedlak and Stypulkowska[19] used ATR-FTIR to identify NPS in illicit samples. Measurements using Raman spectroscopy to characterize NPS are described in some studies.[20-23] Raman spectroscopy proved very useful and has been extensively employed to rapidly determine drug abuse, such as hand luggage control for aircraft passengers.[14,24-28] NMR also has been used in NPS characterization;[29] however, it is an expensive equipment and only laboratories with good financial resources can carry out this analysis.

This work investigates R-NBOMe and R-NBOH extracted from blotter papers donated from the Brazilian Federal Police seizures. Structural and spectroscopic techniques were employed to identify 25R-NBOH (R = Cl, Et), and 25I-NBOMe as the NPS in these samples. Single-crystal X-ray diffraction was applied as a reference technique to determine the crystalline structure of the single crystal obtained from the seized blotter papers extracts. Some of these structures are being reported for the first time in this contribution. This approach is essential to confirm the efficiency of the isolation and extraction process to produce reference standards for the characterization with other experimental methods. Thus, Fourier transform Raman (FT-Raman), ATR-FTIR, and NMR spectroscopies were applied to investigate the molecular structure identified by single X-ray diffraction. This study also used the reference ATR-FTIR spectrum library collected by the Scientific Working Group for the Analysis of Seized Drugs (SWGDRUG) organization.[30]

Experimental

Reagents

Gradient-grade methanol was purchased from Exodus (Sumaré, Brazil), and deuterated methanol was supplied by Cambridge Isotope Laboratories, Inc. (Andover, USA).

Samples and extraction

In this study, 150 blotter papers with approximately 1 cm^2 area, seized between 2020 and 2021 in Brazil, containing 25B-NBOH, 25E-NBOH, 25I-NBOH, 25C-NBOH, and 25I-NBOMe were kindly donated by Federal Police Pequi's Project. The samples were separated into five groups (A, B, C, D and E), based on previous routine analyses, such as GC-MS. Each sample group of 10 blotter paper was submitted to 20 mL methanol extractions, first in an ultrasonic bath for 8 min followed by vortex stirring. Then, powder samples were obtained by slow evaporation at room temperature. The expected molecular structures are shown in Figure 1.

Single crystal X-ray structure determination

Single crystal X-ray diffraction data (ϕ scans and ω scans with κ and θ offsets) were collected on a Bruker D8 Venture (Karlsruhe, Germany) κ-geometry diffractometer equipped with a Photon II CPAD detector and an IμS 3.0 Incoatec Cu Kα (λ = 1.54178 Å) microfocus source. The APEX 4 software[31] was used for unit cell determination and data collection. The data reduction and global cell refinement were done using the Bruker SAINT+ software package,[32]

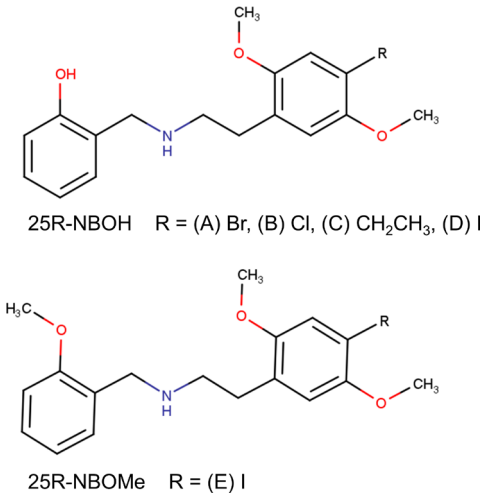

Figure 1. Molecular structures of the 25R-NBOH and 25R-NBOMe.

and a numerical absorption correction was performed with SADABS.[33,34] Using the Olex2 interface program to the SHELX suite,[35] the structure was solved by the intrinsic phasing method implemented in SHELXT,[36] allowing the location of most of the non-hydrogen atoms. The remaining non-hydrogen atoms were located from difference Fourier maps calculated from successive full-matrix least-squares refinement cycles on F^2 with SHELXL[37] and refined using anisotropic displacement parameters. Hydrogen atoms were placed according to geometrical criteria and treated using the riding model. The programs MERCURY[38] and ORTEP-3[39] were used to prepare the artwork representations for publication. The structures of 25B-NBOH and 25I-NBOH had already been reported.[13]

Spectroscopic methods

FT-Raman spectra were recorded using a Bruker RAM II (Karlsruhe, Germany) module equipped with a liquid nitrogen cooled high-sensitivity Ge detector and coupled to a VERTEX 70 FT-IR spectrometer. The samples were excited with the 1064 nm line of a Nd:YAG laser, using a typical resolution of ca. 2 cm^{-1} and a nominal laser power of 150 mW. ATR-FTIR spectra were recorded on a PerkinElmer Spectrum Two spectrometer (Llantrisant, United Kingdom), with a single reflection diamond ATR accessory. Range: 4000-650 cm^{-1}, 16 scans and 4 cm^{-1} resolution. NMR spectra were recorded using a Brucker Avance-DRX 500 spectrometer (Rheinstetten, Germany) at 300 K with 500 MHz for ^1H NMR and 125 MHz for ^{13}C NMR. Assignments were made via ^1H NMR, ^{13}C NMR, ^{13}C-distortionless enhancement by polarization transfer (^{13}C-DEPT), $^1H/^{13}C$-heteronuclear single-quantum correlation spectroscopy ($^1H/^{13}C$-HSQC), using $CDCl_3$ solvent.

Results and Discussion

The 25R-NBOH NPS and 25I-NBOMe synthetic drugs were characterized by single-crystal X-ray diffraction, FTIR, Raman, and multinuclear NMR spectroscopies. All samples were analyzed by single-crystal X-ray diffraction, but 25B-NBOH and 25I-NBOH had already been reported,[13] while 25C-NBOH (Cl), 25E-NBOH (Et), and 25I-NBOMe had not been reported yet. The information provided should be useful in the area of medical, pharmaceutical and forensic applications.

Single-crystal X-ray diffraction

The crystal structures of hydrochloride forms of 25C-NBOH (Cl), 25E-NBOH (Et), and 25I-NBOMe were determined by SCXRD. 25C-NBOH and 25E-NBOH hydrochlorides crystallized in the $P\bar{1}$ space group with one and two molecules *per* asymmetric unit, respectively. On the other hand, 25I-NBOMe crystallized in the $P2_1/c$ space groups as a hydrochloride hydrate with one molecule *per* asymmetric unit. All the crystal data from 25B-NBOH, 25C-NBOH, 25E-NBOH, 25I-NBOH and 25I-NBOMe were analyzed in this study, but 25B-NBOH and 25I-NBOH were first reported by Barros *et al.*,[13] this data were included in this study for comparison. In the Table 1 are presented these crystal data. The asymmetric units of these crystal structures are shown in Figure 2. The determination of the crystalline structure was useful as a reference identification method for synthetic drugs.

Interestingly, all the substituted 25R-NBOH (R ≠ H) crystalline structures are characterized by the same set of

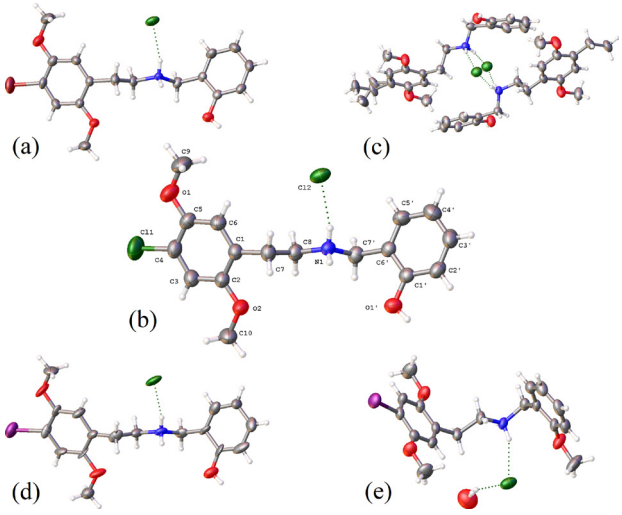

Figure 2. Asymmetric units of 25R-NBOH and 25I-NBOMe crystal structures. The atomic labelling of the common molecular backbone of these compounds is presented in (b). (a) 25B-NBOH, (b) 25Cl-NBOH, (c) 25E-NBOH, (d) 25I-NBOH, (e) 25I-NBOMe.

Table 1. Crystal data of the 25R-NBOH and 25I-NBOMe structures

	A[13]	B	C	D[13]	E
Empirical formula	$C_{17}H_{21}BrNO_3{\cdot}Cl$	$C_{17}H_{21}ClNO_3{\cdot}Cl$	$C_{19}H_{26}NO_3{\cdot}Cl$	$C_{17}H_{21}INO_3{\cdot}Cl$	$C_{18}H_{23}INO_3{\cdot}Cl{\cdot}H_2O$
CCDC number	2031664	2111279	2111278	2031662	2111277
Formula weight / (g mol^{-1})	402.70	358.25	351.86	449.70	481.74
Crystal system	triclinic	triclinic	triclinic	triclinic	monoclinic
Space group	$P\bar{1}$	$P\bar{1}$	$P\bar{1}$	$P\bar{1}$	$P2_1/c$
Z	2	2	2	2	4
Color	colorless	colorless	colorless	colorless	colorless
Habit	plate	prism	prism	needle	block
Unit cell					
a / Å	7.5284(8)	7.5347(7)	7.7122(4)	7.6130(12)	13.5690(4)
b / Å	9.1706(9)	9.1815(10)	15.7470(11)	9.2351(15)	7.4972(2)
c / Å	13.4095(14)	13.4133(16)	17.1118(12)	13.520(3)	21.0252(7)
α / degree	95.399(3)	94.914(7)	111.677(4)	96.483(10)	90
β / degree	93.128(3)	94.510(7)	97.213(4)	90.860(10)	103.0660(10)
γ / degree	103.025(3)	102.759(7)	100.187(4)	103.339(9)	90
Volume / Å^3	895.23(16)	897.14(17)	1858.9(2)	918.2(3)	2083.51(11)
ρ_{calc} / (g cm^{-3})	1.494	1.326	1.257	1.627	1.536
μ / mm^{-1}	2.458	3.368	1.947	1.902	13.432
F(000)	412.0	376.0	752.0	448.0	968.0
Absorption correction	multi-scan	numerical	numerical	multi-scan	numerical
Crystal size / mm^3	0.15 × 0.1 × 0.05	0.407 × 0.197 × 0.07	0.541 × 0.199 × 0.142	0.22 × 0.1 × 0.05	0.462 × 0.259 × 0.2
Radiation	MoKα (λ = 0.71073 Å)	CuKα (λ = 1.54178 Å)	CuKα (λ = 1.54178 Å)	MoKα (λ = 0.71073 Å)	CuKα (λ = 1.54178 Å)
Diffractometer	Bruker APEX-II CCD	Bruker D8 Venture	Bruker APEX-II CCD	Bruker D8 Venture	Bruker D8 Venture
Data collected	33262	39833	13787	5875	83368
Independent reflections	3271	3556	7289	3115	4139
Symmetry factor (R_{int})	0.1290	0.0613	0.0516	0.1592	0.1024
Data/restraints/ parameters	3271/0/208	3556/0/211	7289/12/461	3115/0/208	4139/0/233
Tmin,Tmax	–	0.474,0.790	0.660,0.758	–	0.031,0.087
Goodness-of-fit on F^2	1.029	1.036	1.033	1.022	1.088
Final R_1 for I > 2σ(I)	0.0554	0.0524	0.0650	0.1214	0.0519
wR_2 for all data	0.1161	0.1470	0.1758	0.4019	0.1424
Largest peak/hole / (e Å^{-3})	0.35/–0.54	0.64/–0.30	0.64/–0.30	1.33/–1.83	1.23/–1.26

A: 25B-NBOH; B: 25C-NBOH; C: 25E-NBOH; D: 25I-NBOH; E: 25I-NBOMe; CCDC: Cambridge Crystallographic Data Centre; Z: number of molecules in a unit cell; ρ: density; μ: absorption coefficient; F(000): sum of scattering factors at theta = zero; R1: often called the R-value, is the agreement between the calculated and observed models; I: intensities; σ: statistical uncertainties; wR_2: is similar to R1, but refers to squared F-values.

intermolecular interactions defining the crystal packing. Thus, the chlorine counter-ion holds three hydrogen bonds with different neighboring molecules (Table S1, Supplementary Information (SI) section). Two NH…Cl (3.12-3.20 Å) bonds link the chlorine to the protonated amino groups whereas the latter is associated with the methoxyphenyl group through an OH…Cl bond (3.17-3.22 Å). These bonds arrange molecules into $(25R\text{-}NBOH^{+}{\cdot}Cl^{-})_2$ cyclic tetramers, which could be furtherly stabilized by a C7H…π bond (3.14-3.18 Å) with the methoxyphenyl ring as acceptor (Figure 3). The CH…π interaction are evidenced by the red depressions in the Hirshfeld surface mapped with the shape index.[40] In the case of halogen substitutions, the tetramer is centrosymmetric, but the ethyl disorder in 25E-NBOH suppresses the inversion center leading to the doubling of Z' and Z. The tetramers are linked by the bonds OH…Cl (3.12-3.20 Å), supported by a weak C2'H…Cl for R=halogen, and C10H…π (2.66-2.77 Å), between dimethoxyphenyl rings, forming planes parallel to the bc-plane (Figure S1, SI section). Finally, these planes are stacked along the *a*-axis by weak CH…Cl and CH…O interactions slightly dependent on the substituent.

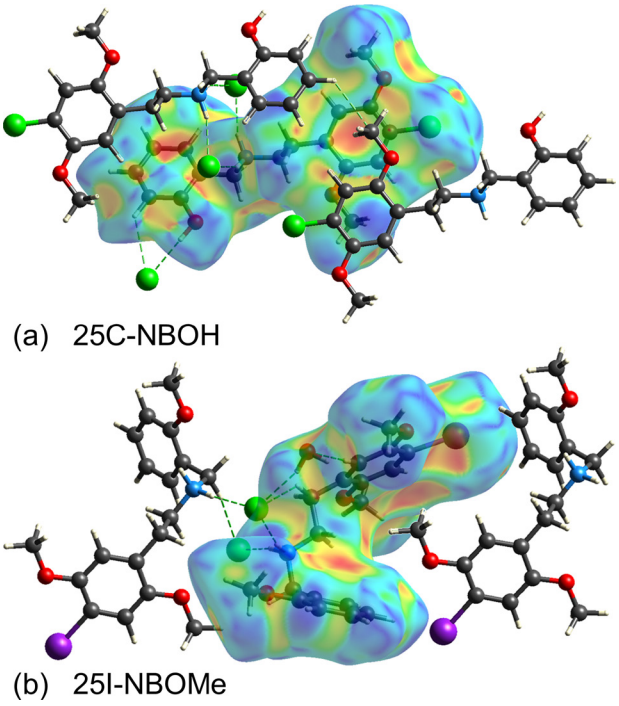

Figure 3. Representative intermolecular interactions of (a) 25R-NBOH and (b) 25I-NBOMe. Strong red depressions on the Hirshfeld surface mapped with the shape index evidence the CH…π interactions.[40]

The comparison of the crystalline structures clearly shows that halogen-substituted 25R-NBOH are isostructural. That is not the case of 25E-NBOH because not only there is the loss of one inversion center due to the ethyl disorder which requires the doubling of the unit cell but also there is a conformational difference between the two non-equivalent molecules. It is also interesting to point out that the structure of the non-substituted 25H-NBOH molecule, reported by Barros *et al.*,[13] differs considerably from the substituted counterparts. The main chlorine-based hydrogen bonds are preserved, but the packing changes do not lead to the organization as a tetramer. This is mainly due to the conformational change of 25H-NBOH, which is characterized by a non-coplanar aminoalkyl chain in opposition to the planar conformation observed in the substituted molecules.

The last benzylphenethylamine derivative investigated in this work was 25I-NBOMe. Despite the molecular similarities with the 25R-NBOH family, a distinctive molecular conformation was observed in the crystal structure of its hydrated salt. Whereas the aminoalkyl chain remains approximately planar, the methoxyphenyl ring is flipped being oriented almost facing the dimethoxyphenyl one. The main intermolecular interactions are the two NH…Cl associated with the protonated amino group. However, instead of forming tetramers, one of these hydrogen bonds, supported by OwH…O5 and OwH…Cl interactions, arrange the molecules in a helical chain around the screw axis along the b-direction (see Table S1). C10H…π interactions also contribute to this chain as observed in Figure 3b. Finally, the helical columns are held together by the second NH…Cl hydrogen bond, as well as C5'H…π and C10H…π linking the methoxyphenyl and dimethoxyphenyl rings (Figure S1). It is also important to point out that this is the first report of the crystalline structure of a member of the 25R-NBOMe group.

Vibrational spectroscopy

Raman spectra were obtained from small crystals of 25R-NBOH (R = Br, Cl, Et, I) and 25I-NBOMe samples to reduce the interference of impurities. Figure 4 exhibited the spectra of 25B-, 25C-, 25E- and 25I-NBOH, whilst Figure 5 shows the comparison between 25I-NBOH and 25I-NBOMe.

Although there has been an attempt to reduce impurities, particularly the 25I-NBOH spectrum presents a large noise in the range of 300 to 600 cm^{-1} that can be attributed to residues of the purification process. For example, these bands are quite present in cellulose, the main constituent of blotter papers.[41] Furthermore, unlike reported in the literature,[29] it is not possible to clearly visualize a double peak at 1250 cm^{-1} related to the substitution by OH of the *N*-benzyl group in Figure 4a. This was probably due to a large amount of impurities present in these samples.

Besides that, it is possible to distinguish the 1250 cm^{-1} band of asymmetric C–O–C of NBOMe in Figure 5b, correlated to OCH_3 substitution of *N*-benzyl group, a characteristic band used in infrared spectroscopy to NBOH and NBOMe identification. In 25I-NBOH spectra, a weak double peak can be noticed and related to OH substitution.[6]

Also, in Figure 4b it is possible to correlate vibrations bands at 1040, 1064 and 1078 cm^{-1} to aryl-I, aryl-Br and aryl-Cl substitutions, respectively.[42] This differentiation is essential to identify which substitute is present in the NBOH group.

As mentioned, despite attempts to reduce impurities, 25R-NBOH and 25I-NBOMe spectra are very complex, therefore this discussion focused on the main differences between these NPS to obtain a sensitive identification method.[43]

ATR-FTIR spectrum of samples A, B, C, D and E groups as in Raman spectrum, also indicated the presence of small impurities that were not eliminated during the extraction processes, attributed to a blotter paint pigment and cellulose. The single infrared spectral profile analysis was performed using reference literature[44] and available forensic libraries such as Europe Response infrared

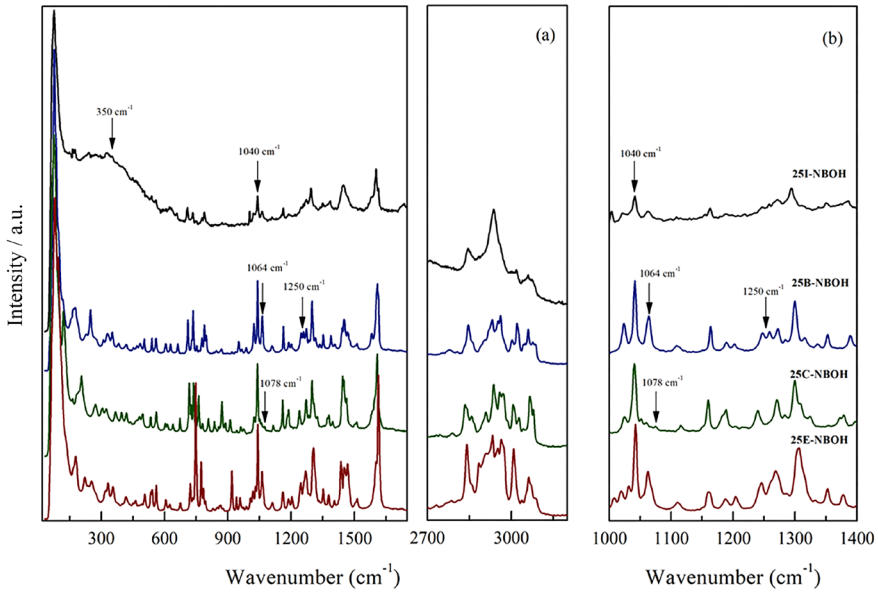

Figure 4. Comparison of Raman spectra for studied 25R-NBOH class. The arrows show the relevant bands. (a) Region 20-1750 cm^{-1} and 2700-3200 cm^{-1}, (b) region 1000-1400 cm^{-1}.

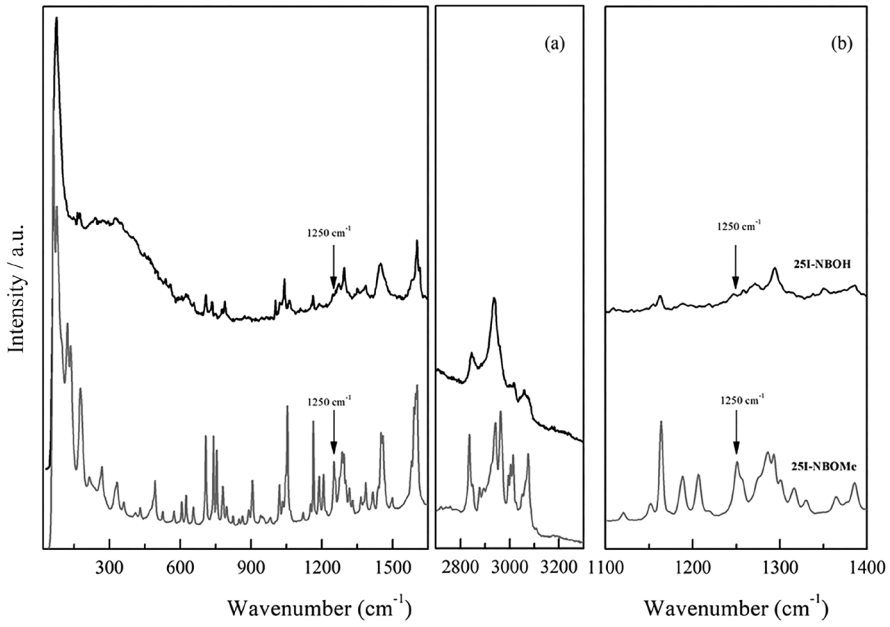

Figure 5. Comparison of Raman spectra of 25I-NBOH and 25I-NBOMe. The arrows indicate the increase of spectral band in 1250 cm^{-1} indicating the substitution of OH by OCH_3. (a) Region 20-1650 cm^{-1} and 2700-3200 cm^{-1}, (b) region 1100-1400 cm^{-1}.

library[45] and SWGDRUG.[46] The profile analysis indicated the presence of signals matching with NBOH drugs. It was observed in 25R-NBOH groups a degree of similarity with 25R-NBOMe, however, it was observed, as in Raman analysis, a decrease of the spectral band centered around 1250 cm^{-1}, characteristic of asymmetric C–O–C vibrations of NBOMe groups, indicated the substitution of OCH_3 by OH.

All the 25R-NBOH FTIR spectrum groups showed similar bands (Table 2). It was observed the presence of intense vibration characteristic of phenol stretch C–O at ca. 1211 cm^{-1}, symmetrical and asymmetric stretches of aryl-alkyl-ethers at 1032-1041 and 1266 cm^{-1}, medium to weak stretch of alkyl-amine C–N at 1109 cm^{-1}. It was also observed strong absorption at a range of 751 to 756 cm^{-1} due to Ar-R (R = Br, Cl, Et, I) deformation. In the 25I-NBOH spectra the band at 751 cm^{-1} was attributed to out-of-plan aromatic C–H deformation. In the spectra of 25B-NBOH, 25C-NBOH and 25E-NBOH, this same peak is slightly displaced, being present, respectively, in the waves number 752, 756 and 750 cm^{-1}, but with lower intensity. Therefore, this band is of fundamental importance in distinguishing the substitute from position 4

Table 2. Assignments of the 25R-NBOHs FTIR main absorption bands

Band	25B-NBOH / cm^{-1}	25C-NBOH / cm^{-1}	25E-NBOH / cm^{-1}	25I-NBOH / cm^{-1}	25I-NBOMe / cm^{-1}	Assignments
1	752	756	750	751	757	Ar-R (R = Br, Cl, Et, I) axial deformation, aromatic ring, disubstituted
2	766	766	766	766	766	aromatic ring, disubstituted
3	1032, 1041, 1266	1032, 1041, 1266	1032, 1041, 1266	1032, 1041, 1266	1032, 1041, 1266	symmetrical and asymmetric stretches of aryl-alkyl-ethers
4	1109	1109	1109	1109	1109	stretch of alkyl-amine C–N
5	1250-1200	1250-1200	1250-1200	1250-1200	1250-1200	axial deformation of C–I
6	ca. 1434	ca. 1434	ca. 1434	ca. 1434	ca. 1434	angular deformation (CH_2)
7	2917-2849	2917-2849	2917-2849	2917-2849	2917-2849	axial deformation of C–H (sp^3)
8	3200-2500	3200-2500	3200-2500	3200-2500	3200-2500	axial deformation of N–H O–H, C–H

of the aromatic ring, for an unequivocal characterization of the ring substitute.

The stretches O–H, C–H and N–H are also represented in the region of 3400-2500 cm^{-1}. Bending vibrations referring to adjacent hydrogens (H) in the disubstituted ring is at 734 cm^{-1}. Figure 6 shows the comparative FTIR reflectance spectrum with the relevant vibrations found in the 25R-NBOH series.

Figure 7 shows a comparison between 25I-NBOH and 25I-NBOMe. It was observed a band overlapped, and bands assigned to impurity substances such as pigment from the art stamp and cellulose. The relevant bands attributed to a 25I-NBOMe sample were observed at 3392 cm^{-1}, which is in the region of 3600-3200 cm^{-1}, assigned to the axial deformation N–H of the amine group, 2836 and 2937 cm^{-1} bands representing the axial strain C–H of carbon sp^3, groups CH_3 and CH_2, the band at 1437 cm^{-1} corresponding to symmetrical angular deformation in the plane of CH_2, the ether group was characterized by the 1020 cm^{-1} band, characterizing the intense axial deformation C–O–C. 756 cm^{-1} band, the disubstituted aromatic ring was identified through the appearance of the band which corresponds to symmetrical angular deformation outside the C–H plane, and the presence of iodine was due to the band 1214 cm^{-1}, corresponding to axial deformation C–I.[47] The main difference between 25I-NBOH and 25I-NBOMe is the band in 1020 cm^{-1} assigned to the axial deformation C–O–C.

NMR studies

The NBOHs are 1,2,4,5-tetra-substituted aromatic ring substituted containing two methoxy, one ethylmethylamine

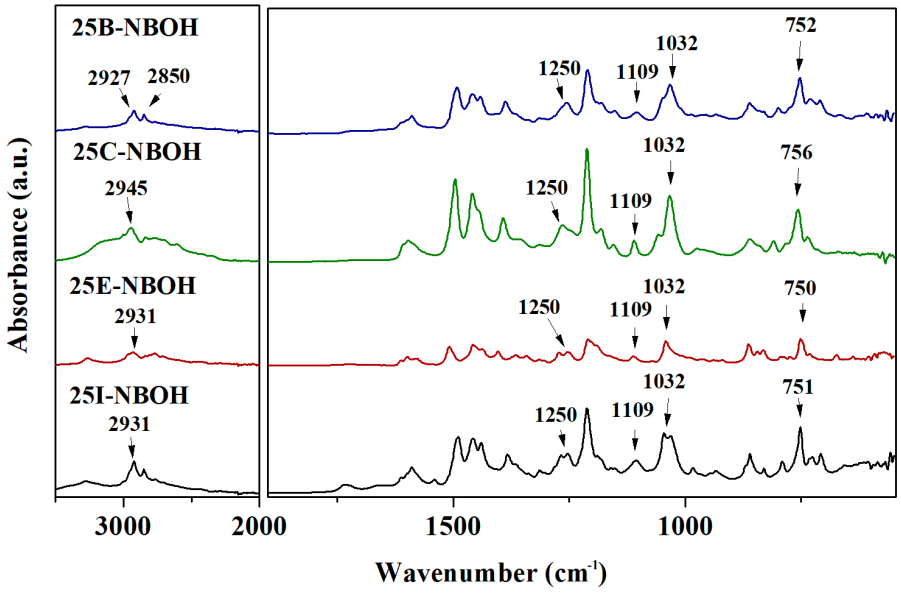

Figure 6. Comparison of ATR-FTIR for 25R-NBOH spectrum.

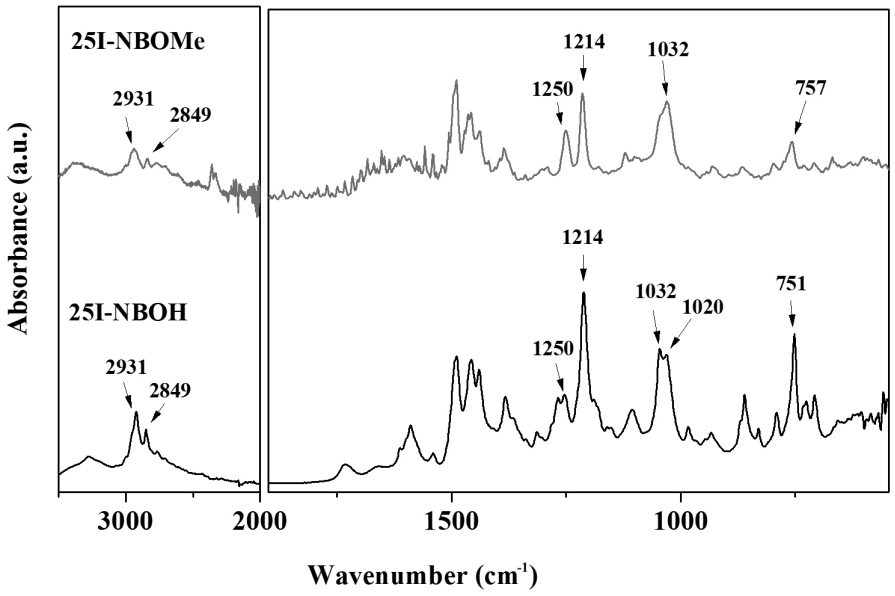

Figure 7. Comparison of ATR-FTIR for 25I-NBOH and 25I-NBOMe spectrum.

group and an alkyl or halogen attached on position-4. The amine group attached to one 1,2-disubstituted aromatic ring that contained one hydroxyl group (Figure 8).

^{1}H, ^{13}C, DEPT 135 and HSQC NMR experiments were used for characterizing the compounds (Tables S2-S4 and Figures S12-S31, SI section). NMR spectroscopic results of C and E are presented in Tables 3 and 4. The Figures 8 and 9 show the complete assignment of ^{1}H NMR spectrum of C and E. It was observed eleven types of H-signal (three of these signals were overlapped) and seventeen types of C-signal for the 25B, 25C and 25I-NBOH; thirteen types of H-signal and nineteen types of C-signal for the 25E-NBOH. Minor impurities were detected in spectrum, especially in the 25I-NBOH, without prejudice to the data interpretation.

To explain the observed chemical shifts, inductive and mesomeric effects in electronic density distribution from the aromatic substitution reaction mechanism can be used. A substitute with a free orbital can increase the electronic

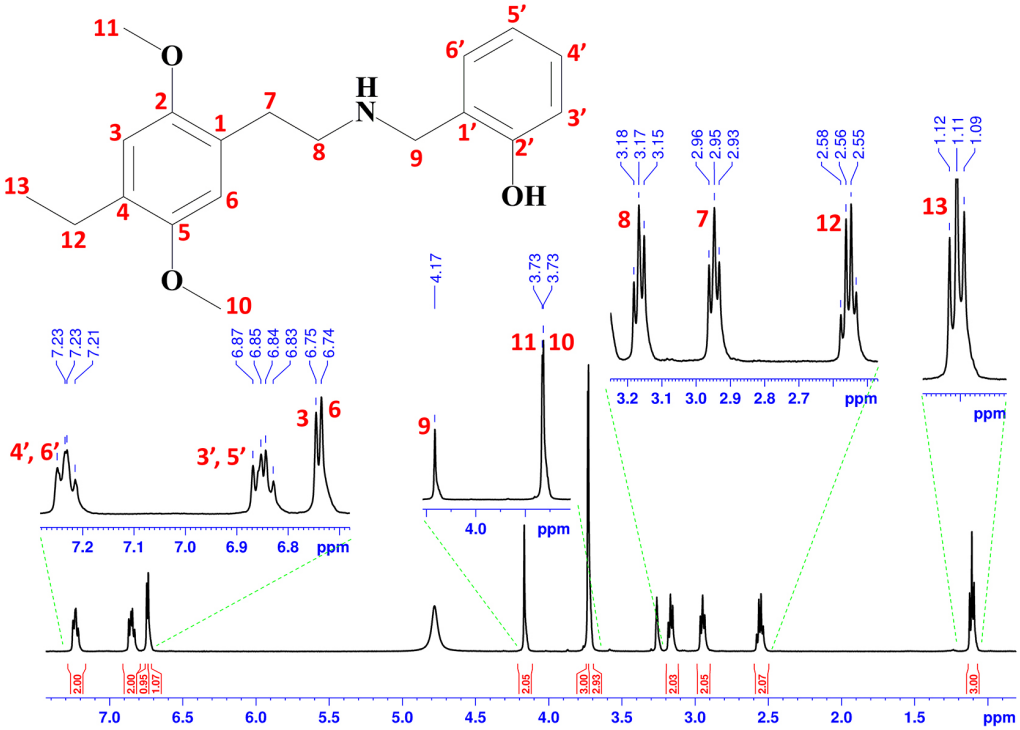

Figure 8. ^{1}H NMR spectrum (500 MHz, methanol-d_4) of compound C (25E-NBOH).

Table 3. ^{1}H and ^{13}C nuclear magnetic resonance (NMR) spectral data for compound C (25E-NBOH) obtained at 500 MHz (methanol-d_4)

Position	^{1}H (δ / ppm, M, J / Hz, integral)	^{13}C δ / ppm	DEPT 135
1	–	126.2	C
2	–	153.4	C
3	6.75, s, 1H	113.6	CH
4	–	n.d.	C
5	–	153.3	C
6	6.74, s, 1H	117.3	CH
7	2.95, t, *J* 7.5, 2H	28.4	CH_2
8	3.17, t, *J* 7.5, 2H	48.4	CH_2
9	4.17, s, 2H	47.9	CH_2
10/11	3.73, s, 3H/3.73, s, 3H	57.6/56.7	CH_3
12	2.56, q, *J* 7.5, 2H	25.9	CH_2
13	1.11, t, *J* 7.5, 3H	12.5	CH_3
1’	–	118.3	C
2’	–	157.5	C
3’	6.87-6.83, m, 1H	116.5	CH
4’	7.23-7.21, m, 1H	132.6	CH
5’	6.87-6.83, m, 1H	121.1	CH
6’	7.23-7.21, m, 1H	132.4	CH

M: multiplicity; *J*: coupling constant; DEPT: distortionless enhancement by polarization transfer; s: singlet; n.d.: not detected; t: triplet; q: quartet; m: multiplet.

Table 4. ^{1}H and ^{13}C nuclear magnetic resonance (NMR) spectral data for compound E (25I-NBOMe) obtained at 500 MHz (methanol-d_4)

Position	^{1}H (δ / ppm, M, J / Hz, integral)	^{13}C δ / ppm	DEPT 135
1	–	127.2	C
2	–	153.8	C
3	7.24, s, 1H	123.5	CH
4	–	85.2	C
5	–	154.6	C
6	6.76, s, 1H	115.3	CH
7	2.91, t, *J* 7.5, 2H	28.6	CH_2
8	3.12, t, *J* 7.5, 2H	47.9	CH_2
9	4.13, s, 2H	48.2	CH_2
10	3.67, s, 3H	56.3	CH_3
11	3.71, s, 3H	56.8	CH_3
12	3.78, s, 3H	57.8	CH_3
1’	–	120.5	C
2’	–	159.4	C
3’	6.98, d, *J* 7.5, 1H	112.5	CH
4’	7.35, t, *J* 7.5, 1H	132.7	CH
5’	6.91 t, *J* 7.5, 1H	122.2	CH
6’	7.27, d, *J* 7.5, 1H	132.7	CH

M: multiplicity; *J*: coupling constant; DEPT: distortionless enhancement by polarization transfer; s: singlet; t: triplet; d: duplet.

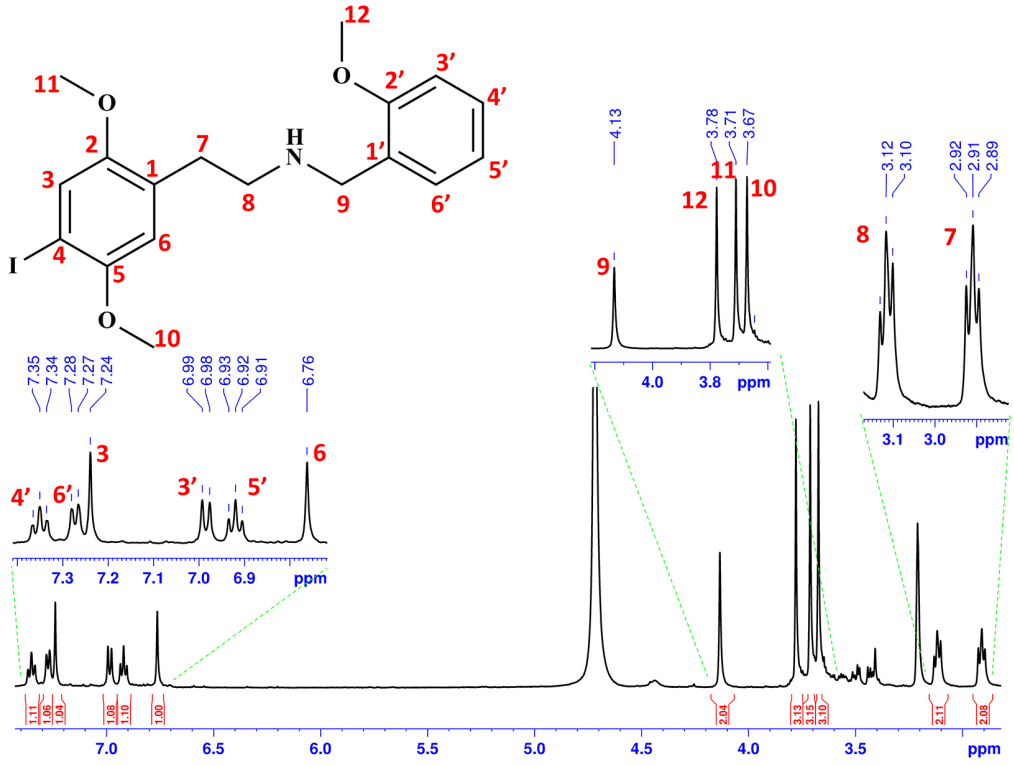

Figure 9. ^{1}H NMR spectrum (500 MHz, methanol-d_4) of compound E (25I-NBOMe).

density in the *ortho* and *para* positions, which leads to a shielding of the corresponding carbon and hydrogen atoms resulting in an upfield shift.[48] Atoms with unshared pairs of electrons as oxygen, nitrogen and halogens have the opposite inductive effect due to the electronegativity exceeded.

This substituent can act both as an electron withdrawing group (due to electronegativity, thus causing a shift to higher frequencies) and as a donor of lone pairs (thus causing a shift to lower frequency). So, the mesomeric effects can be used to explain the shielding observed in halogenate aromatic compounds, in which the protons in the *ortho* and *para* positions are more strongly shielded than in the *meta* position. The effect can be observed when investigated the 25C, 25B and 25I-NBOH, where the proton in the *meta* position (position-6) has smaller chemical shifts compared with proton in the *para* position (position-3). The halogens affect the shielding increases along the series F to I because the halogen electronegativity decreases, presumably leading to more electron density on the atom bound to it. Then, the chemical shift of protons in the *para* position (position-3) increase (7.01 ppm in the 25C, 7.13 ppm in the 25B and 7.33 ppm in the 25I-NBOH). Otherwise, the chemical shift of protons in the *meta* position (position-5) decrease (6.94 ppm in the 25C, 6.92 ppm in the 25B and 6.83 ppm in the 25I-NBOH). The strong shielding observed for the *ipso*-carbon (C-4) confirmed the halogen presence attached directly to aromatic ring. On the other hand, the deshielding of C-2', C-2 and C-5 corroborated the presence of a hydroxyl and methoxy group substituents.

The 25I-NBOH and 25I-NBOMe compounds have a distinctive aromatic carbon, bonded to iodine, at 83-86 ppm. The compounds can be differentiated from number of methyl group attached on aromatic ring, the 25I-NBOH has two signals at 56-58 ppm, while 25I-NBOMe has three.

Conclusions

The Early Warning Systems (EWA) is a reality around the world, so it is very important that researchers apply traditional methods of molecular structure to identify NPS and prohibited synthetic drugs, and in this work the results showed that the single crystal X-ray presents promising results.

The X-ray studies is an unprecedented because the crystalline structures of the hydrochloride salts of 25C-NBOH and 25E-NBOH were reported for the first time in this work. These structures were compared with those of 25B-NBOH.HCl and 25I-NBOH.HCl showing that halide substituted 25R-NBOH salts are isostructural, whereas the 25E-NBOH salt lattice is doubled due to the ethyl moiety disorder but preserves the main features of the 25R-NBOH family. The crystal packing of the substituted compound differs considerably from the unsubstituted one (R = H). Also, the crystalline structure of 25I-NBOMe was determined as a hydrochloride hydrated salt, defining a new crystal packing despite the structural similarities with the 25R-NBOH drugs. It was not possible to compare this structure with other substituted molecules because it was the first report of a crystalline structure of the NBOMe family.

The spectroscopic methods studies (ATR-FTIR, Raman and NMR) confirmed and identified that compound A was (4-bromo-2,5-dimethoxyphenethyl) (2-hydroxybenzyl)amine (25B-NBOH), compound B was (4-chloro-2,5-dimethoxyphenethyl)(2-hydroxybenzyl) amine (25C-NBOH), compound C was (4-ethyl-2,5-dimethoxyphenethyl)(2-hydroxybenzyl)amine (25E-NBOH), compound D was (4-iodo-2,5-dimethoxyphenethyl)(2-hydroxybenzyl)amine (25I-NBOH) and compound E was (4-iodo-2,5-dimethoxyphenethyl) (2-methoxybenzyl)amine (25I-NBOMe). The single crystal X-ray diffraction was used to produce a reference material to match the spectrum and to include in a FTIR database spectrum. SWGDRUG library also was used in FTIR analyses as a reference library.

The single crystal X-ray diffraction is a powerful technique to use as a reference method to forensic purpose because it is a non-destructive method, and it is useful to use the isolated identified crystal as a reference material that could be used in other techniques.

Supplementary Information

Crystallographic data obtained for the structures (25I-NBOMe, 25E-NBOH and 25C-NBOH) in this work were deposited in the Cambridge Crystallographic Data Centre (CCDC) as supplementary publication number CCDC: 2111277-2111279. Copies of the data can be obtained, free of charge, via https://www.ccdc.cam.ac.uk/structures/.

Supplementary information (experimental and characterization details) is available free of charge at http://jbcs.sbq.org.br as PDF file.

Acknowledgments

The authors would like to thank Élvio Botelho (SEPLAB/INC/PF) for samples donation and Centro Nordestino de Aplicação e Uso da Ressonância Magnética Nuclear (CENAUREM) for the NMR experiments. This study was financed in part by the National Police Academy, Fundação

de Amparo à Pesquisa do Estado de Ceará (Funcap) and Coordenação de Aperfeiçoamento de Pessoal de Nível Superior - Brazil (CAPES) - finance code 001 (PROEX 23038.000509/2020-82). Nágila M. P. S. Ricardo thanks CNPq for the research grant (project No. 309795/2021-4).

Author Contributions

Maria C. C. Lucena was responsible for the conceptualization, data curation, formal analysis, funding acquisition, investigation, project administration, writing original draft; Karen P. S. Lopes for the visualization, formal analysis, writing original draft; Alejandro P. Ayala for the formal analysis, writing original draft; Laura M. T. Vidal for the writing original draft; Thiago I. B. Lopes for the formal analysis, writing original draft; Nágila M. P. S. Ricardo for the writing-review and editing, formal analysis, funding acquisition, supervision.

References

1. United Nations Office on Drugs and Crime (UNODC); Synthetic Drug Strategy 2021-2025, https://syntheticdrugs.unodc.org/syntheticdrugs/en/strategy.html, accessed in October 2022.
2. Ferrari Jr., E.; Arantes, L. C.; Salum, L. B.; Caldas, E. D.; *J. Chromatogr. A* **2020**, *1634*, 461657. [Crossref]
3. Ministério da Justiça e Segurança Pública; Relatório de Drogas Sintéticas - 2020, https://www.gov.br/pf/pt-br/acesso-a-informacao/acoes-e-programas/relatorio-de-drogas-sinteticas-2020/relatorio_drogas_sinteticas_2020.pdf/view, accessed in October 2022.
4. Agência Nacional de Vigilância Sanitária (ANVISA); Relatório de Atividades 2017/2018 Grupo de Trabalho para Classificação de Substâncias Controladas (Portaria No. 898/20151), https://www.gov.br/anvisa/pt-br/assuntos/medicamentos/controlados/novas-substancias/arquivos/6669json-file-1, accessed in October 2022.
5. United Nations Office on Drugs and Crime (UNODC); The Role of Drug Analysis Laboratories in Early Warning Systems, https://www.unodc.org/documents/scientific/Drug-Analysis-Systems_EWS_EN.pdf, accessed in October 2022.
6. Custódio, M. F.; Magalhães, L. O.; Arantes, L. C.; Braga, J. W. B.; *J. Braz. Chem. Soc.* **2021**, *32*, 513. [Crossref]
7. Arantes, L. C.; Júnior, E. F.; de Souza, L. F.; Cardoso, A. C.; Alcântara, T. L. F.; Lião, L. M.; Machado, Y.; Lordeiro, R. A.; Neto, J. C.; Andrade, A. F. B.; *Forensic Toxicol.* **2017**, *35*, 408. [Crossref]
8. Coelho Neto, J.; Andrade, A. F. B.; Lordeiro, R. A.; Machado, Y.; Elie, M.; Ferrari Júnior, E.; Arantes, L. C.; *Forensic Toxicol.* **2017**, *35*, 415. [Crossref]
9. United Nations Office on Drugs and Crime (UNODC); What are NPS?, https://www.unodc.org/LSS/Page/NPS, accessed in October 2022.
10. United Nations Office on Drugs and Crime (UNODC); NPS Substance Groups, https://www.unodc.org/LSS/SubstanceGroup/GroupsDashboard?testType=NPS, accessed in October 2022.
11. United Nations; Convention on Psychotropic Substances, 1971, https://www.unodc.org/pdf/convention_1971_en.pdf, accessed in October 2022.
12. United Nations Office on Drugs and Crime (UNODC); Decision 58/3, https://www.unodc.org/documents/commissions/CND/CND_Sessions/CND_58/2015_Desicions/Desicion_58_3.pdf, accessed in October 2022.
13. de Barros, W. A.; Queiroz, M. P.; da Silva Neto, L.; Borges, G. M.; Martins, F. T.; de Fátima, Â.; *Tetrahedron Lett.* **2021**, *66*, 152804. [Crossref]
14. Wood, M. R.; Bernal, I.; Lalancette, R. A.; *Struct. Chem.* **2017**, *28*, 1369. [Crossref]
15. Kuś, P.; Rojkiewicz, M.; Kusz, J.; Książek, M.; Sochanik, A.; *Forensic Toxicol.* **2019**, *37*, 456. [Crossref]
16. Nycz, J. E.; Malecki, G.; Zawiazalec, M.; Pazdziorek, T.; Skop, P.; *J. Mol. Struct.* **2010**, *984*, 125. [Crossref]
17. Nycz, J. E.; Malecki, G.; Zawiazalec, M.; Pazdziorek, T.; *J. Mol. Struct.* **2011**, *1002*, 10. [Crossref]
18. Pereira, L. S. A.; Lisboa, F. L. C.; Coelho Neto, J.; Valladão, F. N.; Sena, M. M.; *Microchem. J.* **2017**, *133*, 96. [Crossref]
19. Piorunska-Sedlak, K.; Stypulkowska, K.; *Forensic Sci. Int.* **2020**, *312*, 110262. [Crossref]
20. Guirguis, A.; Girotto, S.; Berti, B.; Stair, J. L.; *Forensic Sci. Int.* **2017**, *273*, 113. [Crossref]
21. Omar, J.; Slowikowski, B.; Guillou, C.; Reniero, F.; Holland, M.; Boix, A.; *J. Raman Spectrosc.* **2019**, *50*, 41. [Crossref]
22. Rojkiewicz, M.; Kuś, P.; Kusz, J.; Książek, M.; Sochanik, A.; *Forensic Toxicol.* **2020**, *38*, 481. [Crossref]
23. Wilson, N. G.; Raveendran, J.; Docoslis, A.; *Sens. Actuators, B* **2021**, *330*, 129303. [Crossref]
24. McLaughlin, G.; Morris, N.; Kavanagh, P. V.; Power, J. D.; Dowling, G.; Twamley, B.; O'Brien, J.; Talbot, B.; Walther, D.; Partilla, J. S.; Baumann, M. H.; Brandt, S. D.; *Drug Test. Anal.* **2017**, *9*, 358. [Crossref]
25. Penido, C. A. F. O.; Pacheco, M. T. T.; Lednev, I. K.; Silveira, L.; *J. Raman Spectrosc.* **2016**, *47*, 28. [Crossref]
26. Hargreaves, M. D.; Page, K.; Munshi, T.; Tomsett, R.; Lynch, G.; Edwards, H. G. M.; *J. Raman Spectrosc.* **2008**, *39*, 873. [Crossref]
27. West, M. J.; Went, M. J.; *Drug Test. Anal.* **2011**, *3*, 532. [Crossref]
28. Burnett, A. D.; Edwards, H. G. M.; Hargreaves, M. D.; Munshi, T.; Page, K.; *Drug Test. Anal.* **2011**, *3*, 539. [Crossref]
29. Machado, Y.; Coelho Neto, J.; Lordeiro, R. A.; Alves, R. B.; Piccin, E.; *Forensic Toxicol.* **2020**, *38*, 203. [Crossref]
30. Scientific Working Group for the Analysis of Seized Drugs (SWGDRUG); Monographs, https://www.swgdrug.org/monographs.htm, accessed in October 2022.

31. *APEX4 Data Collection software*, version 2021.4-0; Bruker AXS Inc.; Madison, Wisconsin, USA, 2021.
32. *SAINT Data Reduction Software*, version 8.40b; Bruker AXS Inc.; Madison, Wisconsin, USA, 2019.
33. Sheldrick, G. M.; *SADABS. Program for Empirical Absorption Correction*; University of Gottingen, Germany, 1996.
34. Krause, L.; Herbst-Irmer, R.; Sheldrick, G. M.; Stalke, D.; *J. Appl. Crystallogr.* **2015**, *48*, 3. [Crossref]
35. Dolomanov, O. V.; Bourhis, L. J.; Gildea, R. J.; Howard, J. A. K.; Puschmann, H.; *J. Appl. Crystallogr.* **2009**, *42*, 339. [Crossref]
36. Sheldrick, G. M.; *Acta Crystallogr., Sect. A: Found. Adv.* **2015**, *A71*, 3. [Crossref]
37. Sheldrick, G. M.; *Acta Crystallogr., Sect. C: Struct. Chem.* **2015**, *C71*, 3. [Crossref]
38. MacRae, C. F.; Sovago, I.; Cottrell, S. J.; Galek, P. T. A.; McCabe, P.; Pidcock, E.; Platings, M.; Shields, G. P.; Stevens, J. S.; Towler, M.; Wood, P. A.; *J. Appl. Crystallogr.* **2020**, *53*, 226. [Crossref]
39. Farrugia, L. J.; *J. Appl. Crystallogr.* **1997**, *30*, 565. [Crossref]
40. Spackman, P. R.; Turner, M. J.; McKinnon, J. J.; Wolff, S. K.; Grimwood, D. J.; Jayatilaka, D.; Spackman, M. A.; *J. Appl. Crystallogr.* **2021**, *54*, 1006. [Crossref]
41. Magalhães, L. O.; Arantes, L. C.; Braga, J. W. B.; *Microchem. J.* **2019**, *144*, 151. [Crossref]
42. Pein, B. C.; Seong, N.-H.; Dlott, D. D.; *J. Phys. Chem. A* **2010**, *114*, 10500. [Crossref]
43. de Andrade, A. F. B.; Gonzalez-Rodriguez, J.; *Analyst* **2019**, *144*, 2965. [Crossref]
44. Pavia, D. L.; Lampman, G. M.; Kriz, G. S.; Vyvyan, J. R.; *Introdução à Espectroscopia*; 4th ed.; CENGAGE Learning: Bellingham, 2010.
45. Republic of Slovenia, Ministry of the Interior; Forensic Drugs Analyses - European project RESPONSE, https://www.policija.si/eng/about-the-police/organization/general-police-directorate/national-forensic-laboratory/project-response, accessed in October 2022.
46. Scientific Working Group for the Analysis of Seized Drugs (SWGDRUG); SWGDRUG IR Library Version 2.1, https://swgdrug.org/ir.htm, accessed in October 2022.
47. dos Santos, P. F.; Souza, L. M.; Merlo, B. B.; Costa, H. B.; Tose, L. V.; Santos, H.; Vanini, G.; Machado, L. F.; Ortiz, R. S.; Limberger, R. P.; Vaz, B. G.; Romão, W.; *Quim. Nova* **2016**, *39*, 229. [Crossref]
48. Holzgrabe, U.; Diehl, B.; Wawer, I.; *NMR Spectroscopy in Pharmaceutical Analysis*; Elsevier, 2008. [Crossref]

Submitted: May 20, 2022
Published online: October 19, 2022